Scaling study of the step scaling function in SU(3) gauge theory with improved gauge actions

doi: 10.1103/PhysRevD.70.074510

Scaling study of the step scaling function in SU(3) gauge theory with improved gauge actions

S. Takeda,[1] S. Aoki,[1] M. Fukugita,[3] K-I. Ishikawa,[5] N. Ishizuka,[1,2] Y. Iwasaki,[1] K. Kanaya,[1] T. Kaneko,[4] Y. Kuramashi,[1,2] M. Okawa,[5] Y. Taniguchi,[1,2] A. Ukawa,[1,2] and T. Yoshié[1,2]

(CP-PACS Collaboration)

[1]*Graduate School of Pure and Applied Sciences, University of Tsukuba, Tsukuba, 305-8571, Japan*
[2]*Center for Computational Sciences, University of Tsukuba, Tsukuba, 305-8577, Japan*
[3]*Institute for Cosmic Ray Research, University of Tokyo, Kashiwa 277-8582, Japan*
[4]*High Energy Accelerator Research Organization (KEK), Tsukuba, Ibaraki 305-0801, Japan*
[5]*Department of Physics, Hiroshima University, Higashi-Hiroshima, Hiroshima 739-8526, Japan*
(Received 10 August 2004; published 19 October 2004)

We study the scaling behavior of the step scaling function for SU(3) gauge theory, employing the renormalization-group improved Iwasaki gauge action and the perturbatively improved Lüscher-Weisz gauge action. We confirm that the step scaling functions from the improved gauge actions agree with that previously obtained from the plaquette action within errors in the continuum limit at both weak and strong coupling regions. We also investigate how different choices of boundary counterterms for the improved gauge actions affect the scaling behavior. In the extrapolation to the continuum limit, we observe that the cutoff dependence becomes moderate for the Iwasaki action, if a perturbative reduction of scaling violations is applied to the simulation results. We also measure the low energy scale ratio with the Iwasaki action and confirm its universality.

DOI: 10.1103/PhysRevD.70.074510 PACS numbers: 11.15.Ha, 12.38.Gc

I. INTRODUCTION

The strong coupling constant is one of the fundamental parameters of QCD. The current world average leads to $\alpha_{\overline{\rm MS}}(m_Z) = 0.1172(20)$ [1]. Lattice QCD calculations have a potential ability to determine the strong coupling constant from an experimental input at low energy scales. In practice, however, one must relate the high energy perturbative QCD scale to the low energy hadronic scale. The Alpha Collaboration proposed the Schrödinger functional (SF) scheme as a vehicle for this purpose [2,3], and it has been successfully applied to lattice QCD in various aspects [4–7]. One of the most recent results related to our study is the running coupling constant of two massless flavor QCD reported in Refs. [8,9].

Recently the CP-PACS and JLQCD Collaborations have started a project for $N_{\rm f} = 3$ QCD simulations [10–14]. These simulations are essential to understand the low energy QCD dynamics for the real world in which three light quarks exist. One of the targets of the project is to evaluate the strong coupling constant $\alpha_{\overline{\rm MS}}$ in $N_{\rm f} = 3$ QCD using the SF scheme. In the project Iwasaki gauge action [15] is employed to avoid the strong lattice artifacts of the plaquette gauge action found in $N_{\rm f} = 3$ simulations [11].

In a previous study [16], as our first step toward evaluation of $\alpha_{\overline{\rm MS}}$ for $N_{\rm f} = 3$, O(a) boundary improvement coefficients in the SF scheme have been determined for various improved gauge actions up to one-loop order in perturbation theory. In addition the scaling violation in the step scaling function (SSF) for the coupling has been analyzed perturbatively. In the present paper, as the next step, we investigate the lattice cutoff dependence of the SSF nonperturbatively in quenched lattice QCD simulations with improved gauge actions. The renormalization-group improved Iwasaki gauge action and the perturbatively improved Lüscher-Weisz gauge action are employed. We investigate the effect of various choices for boundary improvement coefficients in detail, to find the best choice, which will be used in our unquenched simulations in the future. We also confirm the universality of the SSF and the low energy scale ratio, by comparing our results with the previous ones obtained by the ALPHA Collaboration [17,18].

The rest of this paper is organized as follows. In Sec. II, after a brief introduction of the SF scheme and its extension to improved gauge actions, we specify the action and the O(a) boundary improvement coefficients used in our simulations. We then define the Schrödinger functional coupling constant, the step scaling function, and the low energy scale ratio. In Sec. III, we give details of simulations and present our results with improved gauge actions for various choices for O(a) improvement. In Sec. IV, we investigate the lattice cutoff dependence of the step scaling function and the low energy scale ratio, and carefully take the continuum limit of these quantities, in order to confirm their universality. Our conclusion is given in the last section, together with a discussion toward $N_{\rm f} = 2$ and 3 simulations.

II. PRELIMINARIES

A. Schrödinger functional

The SF scheme introduced by the ALPHA Collaboration is a powerful tool to probe the energy evolution of physical quantities. In the SF scheme, the theory is defined on a finite box of size $L^3 \times T$ with the periodic boundary condition in the spatial directions and the Dirichlet boundary condition in the time direction. We set $T = L$ throughout this paper. In the pure SU(3) gauge theory with Wilson plaquette action $S[U]$, the Schrödinger functional is given by

$$\mathcal{Z} = \int D[U] e^{-S[U]}, \tag{2.1}$$

where the link variables $U(x, \mu)$ for the gauge fields satisfy the boundary conditions

$$U(x, k)|_{x_0=0} = \exp\{aC\}, \qquad U(x, k)|_{x_0=L} = \exp\{aC'\}. \tag{2.2}$$

Here a is the lattice spacing, and C and C' are spatially constant diagonal matrices, which depend on the background field parameters η and ν [19].

An extension of the SF scheme to the improved gauge actions was first discussed by Klassen [20] in terms of a transfer matrix construction [21]. In this formulation, each boundary consists of two time slices, to achieve the tree-level O(a^2) improvement.

In this paper, however, we adopt an alternative formulation [22], which achieves the tree-level O(a) improvement with only one time slice at each boundary. The dynamical variables to be integrated over are independent of the form of the action, whether plaquette or improved, and consist of the spatial link variables $U(x, k)$ with $x_0 = a, \ldots, L - a$ and temporal link variables $U(x, 0)$ with $x_0 = 0, \ldots, L - a$ on the cylinder with volume $L^3 \times L$. This formulation is implemented more easily in numerical simulations.

B. Gauge action and O(a) boundary improvement coefficients

The improved action we employ includes the plaquette and rectangle loops and is given by

$$S_{\text{imp}}[U] = \frac{1}{g_0^2} \sum_{C \in S_0} W_0(C, g_0^2) 2\mathcal{L}(C) + \frac{1}{g_0^2} \sum_{C \in S_1} W_1(C, g_0^2) 2\mathcal{L}(C), \tag{2.3}$$

with

$$\mathcal{L}(C) = \text{ReTr}[I - U(C)], \tag{2.4}$$

where W_i is a weight factor to be specified later and $U(C)$ is an ordered product of the link variables along a loop C contained in a set S_0 (plaquette) or S_1 (rectangular). S_0 and S_1 consist of all loops of the given shape which can be drawn on the cylindrical lattice with the volume $L^3 \times L$. The loops involve the "dynamical links" in the sense specified above and spatial links on the boundaries at $x_0 = 0$ and $x_0 = L$. In particular, rectangles protruding from the boundary of the cylinder are not included.

One needs to choose the weight factors appropriately to achieve the one-loop level O(a) improvement. Among various possible choices, ours is given as follows:

$$W_0(C, g_0^2) = \begin{cases} c_0 c_s(g_0^2) \text{ for } C \in P_s: & \text{Set of plaquettes that lie completely on one of the boundaries,} \\ c_0 c_t^P(g_0^2) \text{ for } C \in P_t: & \text{Set of plaquettes that just touch one of the boundaries,} \\ c_0 \text{ for } C \in P_{\text{other}}: & \text{otherwise.} \end{cases} \tag{2.5}$$

$$W_1(C, g_0^2) = \begin{cases} 0 \text{ for } C \in R_s: & \text{Set of rectangles that lie completely on one of the boundaries,} \\ c_1 c_t^R(g_0^2) \text{ for } C \in R_t^2: & \text{Set of rectangles that have exactly two links on a boundary,} \\ c_1 \text{ for } C \in R_{\text{other}}: & \text{otherwise,} \end{cases} \tag{2.6}$$

with

$$c_0 c_t^P(g_0^2) = c_0[1 + c_t^{P(1)} g_0^2 + O(g_0^4)], \tag{2.7}$$

$$c_1 c_t^R(g_0^2) = c_1[3/2 + c_t^{R(1)} g_0^2 + O(g_0^4)], \tag{2.8}$$

where the coefficients c_0 and c_1 of the improved gauge action are normalized such that $c_0 + 8c_1 = 1$. In this paper we consider not only the Iwasaki action ($c_1 = -0.331$, $c_2 = c_3 = 0$) [15] but also the Lüscher-Weisz (LW) action ($c_1 = -1/12$, $c_2 = c_3 = 0$) [23] for comparison, since our perturbative analysis [16] shows that the LW action has a fairly small lattice artifact in the step scaling function. We call $c_t^P(g_0^2)$ and $c_t^R(g_0^2)$ O(a) boundary improvement coefficients. The assignments at the $t = 0$ boundary are shown in Fig. 1. The leading term of the O(a) boundary improvement coefficients in Eqs. (2.7) and (2.8) can uniquely be determined from two requirements that the tree-level O(a) improvement is achieved and the lattice background field satisfies the equation of motion at the boundaries [22]. On the other hand, for the one-loop boundary terms, we can freely set a relation between $c_t^{P(1)}$ and $c_t^{R(1)}$, since there is only one requirement for the one-loop O(a) improvement.

Let us see how we specify the one-loop boundary terms. In Ref. [16], one finds the following relation to achieve the one-loop O(a) improvement:

$$c_0 c_t^{P(1)} + 4c_1 c_t^{R(1)} = A_1/2, \tag{2.9}$$

where A_1 is the coefficient of the a/L term in the one-loop correction $m_1^{(0)}(L/a)$ to the SF coupling. In our simulations we consider two choices: one called condition A is given by

$$c_t^{R(1)} = 2c_t^{P(1)}, \tag{2.10}$$

and the other called condition B is specified by

$$c_t^{R(1)} = 0. \tag{2.11}$$

The difference between conditions A and B is an O(a^5) contribution in the one-loop correction to the SF coupling [16]. Although this difference is tiny at one-loop order, it may become larger at higher orders. The values of one-loop boundary terms for each condition and A_1 are given in Table I. For the LW action, the difference between the two conditions is small, so we do not carry out simulations with condition B.

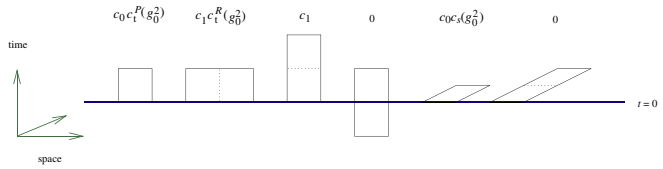

FIG. 1 (color online). The assignments of the weight factor for loops near the boundary $t = 0$ Eqs. (2.5) and (2.6).

C. Schrödinger functional coupling

The SF with the improved gauge action is given by

$$\mathcal{Z} = e^{-\Gamma} = \int D[U] e^{-S_{\rm imp}[U]}, \tag{2.12}$$

where we impose the same boundary condition Eq. (2.2) for the link variables as in the case of the Wilson plaquette action. The SF coupling is defined through the free energy Γ in Eq. (2.12)

$$\bar{g}^2_{\rm SF}(L) = k/\Gamma'|_{\eta=\nu=0} = k/\left\langle \frac{\partial S}{\partial \eta} \right\rangle \Big|_{\eta=\nu=0}, \tag{2.13}$$

where k is a normalization constant

$$k = 12\left(\frac{L}{a}\right)^2 [c_0(\sin 2\gamma + \sin\gamma) + 4c_1(\sin 4\gamma + \sin 2\gamma)], \tag{2.14}$$

$$\gamma = \left(\frac{a}{L}\right)^2 \left(\eta + \frac{\pi}{3}\right). \tag{2.15}$$

The renormalized coupling $\bar{g}^2_{\rm SF}(L)$ depends only on the scale determined by the box size L. The η derivative of the loop touching the boundaries (the leftmost three loops in Fig. 1, for example) contributes to the observable $\partial S/\partial\eta$ in Eq. (2.13).

D. Step scaling function and low energy scale ratio

The SSF describes the evolution of the renormalized coupling under a finite rescaling factor s (we take $s = 2$ in the following):

$$\sigma(2, u) = \bar{g}^2(2L)|_{\bar{g}^2(L)=u}. \tag{2.16}$$

By choosing the $n + 1$th initial value of $\sigma(2, u_{n+1})$ such that $u_{n+1} = \sigma(2, u_n)$, the nonperturbative evolution of the running coupling can be constructed successively in order to cover a wide range of the energy scale.

The SSF $\sigma(2, u)$ in the continuum theory is obtained by the continuum limit of a lattice SSF $\Sigma(2, u, a/L)$

$$\sigma(2, u) = \lim_{a/L \to 0} \Sigma(2, u, a/L). \tag{2.17}$$

In this paper, we study the SSF at a weak coupling $u = 0.9944$ and a strong coupling $u = 2.4484$, where our results can be compared with those of the ALPHA Collaboration.

To fix the scale in a physical unit, one needs to relate the box size L prescribed at a certain value $\bar{g}^2_{\rm SF}(L)$ to some reference scale. Following the conventional way, we set $L = L_{\rm max}$ defined implicitly

TABLE I. The values of $c_t^{P(1)}$ and A_1 for the improved gauge actions with each condition.

Action	$c_t^{P(1)}$ with condition A	$c_t^{P(1)}$ with condition B	A_1
Iwasaki	0.1518	0.04161	0.3036
LW	−0.00297		−0.00594

$$\bar{g}^2_{\rm SF}(L_{\rm max}) = 3.480, \tag{2.18}$$

and adopt Sommer's scale r_0 [24] as the reference scale. Eventually this amounts to computing the ratio $L_{\rm max}/r_0$ and extrapolating it to the continuum limit

$$L_{\rm max}/r_0 = \lim_{a/L_{\rm max}\to 0} (L_{\rm max}/a) \times (a/r_0). \tag{2.19}$$

III. SIMULATION DETAILS AND RESULTS

We follow the calculation procedure of Ref. [19]. Simulations for the SSF on larger lattices are performed on CP-PACS using four partitions of 64 PU's (processor unit), while r_0/a are calculated with two partitions of 512 PU's.

As mentioned in Sec. II C, the SF coupling is obtained by calculating the observable $\partial S/\partial\eta$ for gauge configurations with the SF boundary condition. When the number of spatial lattice points, L/a, is a multiple of 4, the gauge configurations are generated by a combined five-hit pseudo-heat-bath (HB) algorithm and an overrelaxation (OR) algorithm. The combination of one pseudo-heat-bath update sweep followed by $N_{\rm OR} = L/2a$ overrelaxation sweeps is called an iteration. The measurement is implemented after each sweep, i.e., $(1 + L/2a)$ measurements are made per one iteration. Because of a restriction of the HB method optimized for the improved gauge action on CP-PACS, we employ the hybrid Monte Carlo (HMC) algorithm for L/a being different from multiples of 4, for instance $L/a = 6$. The step size for the molecular dynamics is adjusted to achieve an acceptance rate in the range from 0.7 to 0.8. The measurement is made for every trajectory.

Our computations for the renormalized coupling $\bar{g}^2_{\rm SF}(L)$ are carried out on lattices $L/a = 4$, 6, 8, and 12. In this calculation, a reweighting technique is used for a tuning of β [25] such that $\bar{g}^2_{\rm SF}(L)$ becomes a certain prescribed value u for each L/a. And then, using the same β, a computation on a lattice with twice the linear size $2L/a$ gives $\bar{g}^2_{\rm SF}(2L)$. The results are summarized in Tables II and III for the weak ($u = 0.9944$) and the strong ($u = 2.4484$) couplings, respectively. Errors in both $\bar{g}^2_{\rm SF}(L)$ and $\bar{g}^2_{\rm SF}(2L)$ are estimated by a jackknife method. The bin size for jackknife errors is 100 iterations for the HB and 500 trajectories for HMC, respectively. The precision in $\bar{g}^2_{\rm SF}(L)$ is attained by accumulating around

TABLE II. Results of SSF at the weak coupling $u = 0.9944$.

Action	Degree of O(a) improvement	L/a	β	$\bar{g}^2_{\rm SF}(L)$	$\bar{g}^2_{\rm SF}(2L)$	$\Sigma(2, u, a/L)$
	Tree	4	6.5447	0.9944(5)	1.0953(14)	1.0953(16)
		6	6.8485	0.9944(8)	1.0915(19)	1.0915(21)
		8	7.0733	0.9944(12)	1.0973(27)	1.0973(31)
		12	7.3765	0.9944(18)	1.0989(53)	1.0989(57)
Iwasaki		4	6.1467	0.9944(5)	1.1395(16)	1.1395(17)
	One-loop	6	6.5930	0.9944(8)	1.1230(21)	1.1230(24)
	condition A	8	6.8799	0.9944(13)	1.1192(29)	1.1192(33)
		12	7.2547	0.9944(14)	1.1132(40)	1.1132(43)
		4	6.2258	0.9944(5)	1.1284(15)	1.1284(16)
	One-loop	6	6.6358	0.9944(9)	1.1147(22)	1.1147(24)
	condition B	8	6.9010	0.9944(9)	1.1133(30)	1.1133(31)
		12	7.2722	0.9944(15)	1.1134(56)	1.1134(58)
LW	Tree	4	8.2189	0.9944(4)	1.1177(12)	1.1177(13)
		6	8.5889	0.9944(7)	1.1128(17)	1.1128(19)
		8	8.8479	0.9944(10)	1.1136(27)	1.1136(30)
		12	9.2017	0.9944(16)	1.1122(32)	1.1122(37)
		4	8.2199	0.9944(4)	1.1158(12)	1.1158(13)
	One-loop	6	8.5957	0.9944(7)	1.1115(17)	1.1115(19)
	condition A	8	8.8406	0.9944(10)	1.1153(27)	1.1153(30)
		12	9.2060	0.9944(16)	1.1085(47)	1.1085(51)

TABLE III. Results of SSF at the strong coupling $u = 2.4484$.

Action	Degree of O(a) improvement	L/a	β	$\bar{g}^2_{\rm SF}(L)$	$\bar{g}^2_{\rm SF}(2L)$	$\Sigma(2, u, a/L)$
	Tree	4	3.2663	2.4484(28)	3.332(11)	3.332(12)
		6	3.5754	2.4484(52)	3.352(16)	3.352(18)
		8	3.7872	2.4484(40)	3.361(24)	3.361(25)
		12	4.0996	2.4484(65)	3.396(43)	3.396(44)
Iwasaki		4	2.9628	2.4484(29)	4.008(21)	4.008(21)
	One-loop	6	3.3803	2.4484(60)	3.692(21)	3.692(23)
	condition A	8	3.6544	2.4484(42)	3.625(27)	3.625(28)
		12	4.0091	2.4484(68)	3.512(45)	3.512(46)
		4	3.0624	2.4484(29)	3.712(15)	3.712(16)
	One-loop	6	3.4395	2.4484(56)	3.573(20)	3.573(21)
	condition B	8	3.6908	2.4484(47)	3.519(28)	3.519(29)
		12	4.0283	2.4484(64)	3.518(38)	3.518(39)
LW	Tree	4	4.8992	2.4484(24)	3.619(13)	3.619(14)
		6	5.2786	2.4484(49)	3.540(18)	3.540(20)
		8	5.5325	2.4484(42)	3.486(23)	3.486(24)
		12	5.8878	2.4484(62)	3.468(32)	3.468(33)
		4	4.9055	2.4484(25)	3.601(13)	3.601(13)
	One-loop	6	5.2784	2.4484(51)	3.530(18)	3.530(19)
	condition A	8	5.5332	2.4484(40)	3.499(26)	3.499(26)
		12	5.8867	2.4484(58)	3.463(25)	3.463(27)

120 000–140 000 iterations on the lattices $L/a = 4$, 8, and 12, and 300 000 trajectories on the lattices $L/a = 6$. As for $\bar{g}^2_{\rm SF}(2L)$, the number of iterations is around 40 000–80 000 to achieve their precision. Errors in $\bar{g}^2_{\rm SF}(L)$ are propagated into $\Sigma(2, u, a/L)$, the lattice SSF, where u is the central value of $\bar{g}^2_{\rm SF}(L)$. A formula of the error propagation using a perturbative expansion of the SSF can be found in Ref. [26].

We performed an additional set of simulations with the Iwasaki action to determine the low energy scale. The tuning of β to the conventional point $\bar{g}^2_{\rm SF}(L_{\rm max}) = 3.480$ and the error analysis are made in the same way as mentioned above. In Table IV we list the results, which will be used in Sec. IV B as the first factor on the right-hand side of Eq. (2.19). To complete the scale determination, one needs the second factor in Eq. (2.19). In addition to the previous results of r_0/a [27–29], we carried out simulations at $\beta = 3.00$ and 3.53 to cover the range of β in Table IV. Analysis procedures for the static quark potential and extraction of r_0/a parallel those in Ref. [29]. The simulation parameters and results in this work are shown in Table V. To avoid finite size effects, we followed a criterion [18] that the parameter β and L/a are chosen such that $L/r_0 \sim 3.3$. Following the above reference, the number of overrelaxation sweeps are taken to satisfy $N_{\rm OR} \sim 1.5(r_0/a)$.

TABLE IV. Tuning of β at $u = 3.480$ for the Iwasaki action.

Degree of O(a) improvement	$L_{\rm max}/a$	β	$\bar{g}^2_{\rm SF}(L_{\rm max})$
Tree	4	2.7000	3.480(6)
	6	3.0057	3.480(11)
	8	3.2154	3.480(11)
	12	3.5219	3.480(13)
	4	2.4594	3.480(7)
One-loop	6	2.8556	3.480(14)
condition A	8	3.1047	3.480(11)
	12	3.4496	3.480(16)
	4	2.5382	3.480(6)
One-loop	6	2.8921	3.480(11)
condition B	8	3.1376	3.480(12)
	12	3.4734	3.480(14)

IV. CONTINUUM EXTRAPOLATION

A. Step scaling function

In this subsection we investigate the cutoff dependence of the SSF and perform the continuum extrapolation

$$\sigma(2, u) = \lim_{a/L \to 0} \Sigma(2, u, a/L). \tag{4.1}$$

TABLE V. Simulation parameters and results performed in this work for r_0/a with the Iwasaki action. $N_{\rm OR}$ and $N_{\rm conf}$ indicate the number of overrelaxation sweep and configuration, respectively.

β	$(L/a)^4$	r_0/a	$N_{\rm OR}$	$N_{\rm conf}$
3.00	32^4	8.88(13)	15	400
3.53	56^4	17.35(13)	24	88

The lattice SSF $\Sigma(2, u, a/L)$ as a function of a/L at the weak coupling $u = 0.9944$ is shown in Figs. 2(a) and 2(c) for the Iwasaki action and LW action, respectively. For the Iwasaki action, even after the one-loop O(a) improvement with either condition A or condition B, the scaling violation is still rather large, which makes the extrapolation to the continuum limit difficult. To improve the scaling behavior of the SSF, we apply a perturbative removal of the lattice artifacts suggested in Ref. [30] given by

$$\Sigma_1^{(k)}(2, u, a/L) = \frac{\Sigma^{(k)}(2, u, a/L)}{1 + \delta_1^{(k)}(a/L)u}, \tag{4.2}$$

where $\Sigma^{(k)}(2, u, a/L)$ is the SSF (simulation raw data) with the "k"-level O(a) improvement coefficient (e.g., $k = 0$: tree-level $O(a)$ improvement case, $k = 1A$: one-loop $O(a)$ improvement with condition A case, etc.). $\delta_1^{(k)}(a/L)$ is the one-loop relative deviation, given by

$$\delta^{(k)}(2, u, a/L) = \frac{\Sigma^{(k)}(2, u, a/L) - \sigma(2, u)}{\sigma(2, u)} = \delta_1^{(k)}(2, a/L)u + O(au^2), \tag{4.3}$$

whose numerical values are given in Table VI. This method eliminates not only O(a) but also O(a^n) with $n > 1$ lattice artifacts at one-loop order. Figure 2(b) shows the cutoff dependence of $\Sigma_1^{(k)}(2, u, a/L)$. Indeed the scaling violations are much reduced by this method, so that we can reliably take the continuum extrapolation linearly in a as

$$\Sigma_1^{(k)}(2, u, a/L) = \sigma^{(k)}(2, u) + \omega_1^{(k)}(u)a/L, \tag{4.4}$$

where $\sigma^{(k)}(2, u)$ and $\omega_1^{(k)}(u)$ are fit parameters. In Table VII we quote the extrapolated value for the Iwasaki action, which is obtained by a simultaneous fit for $k = 0$, $1A$, and $1B$ data with the constraint that they

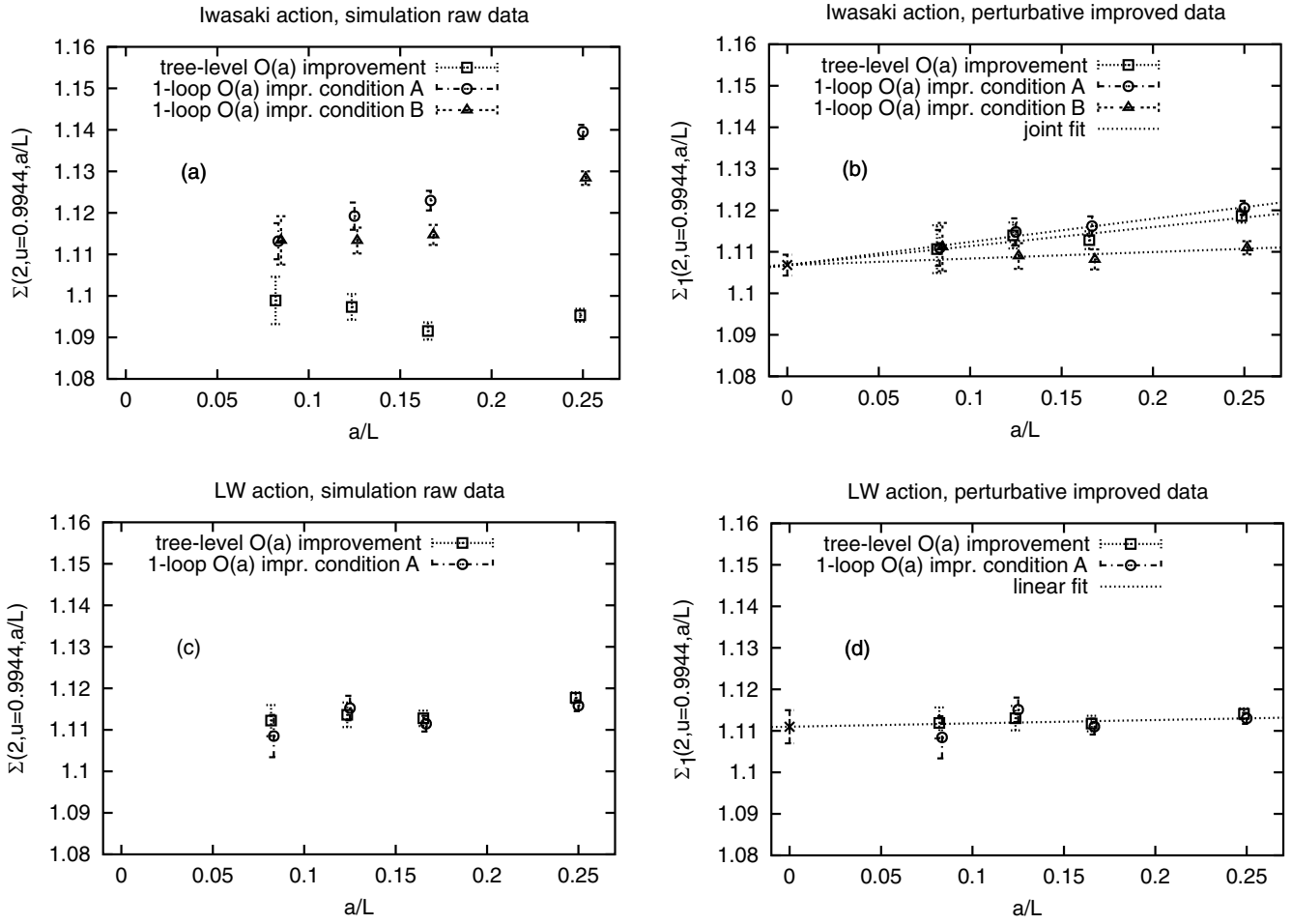

FIG. 2. Results of SSF at the weak coupling $u = 0.9944$ with the Iwasaki action (upper panels) and LW action (lower panels). The simulation raw data (left-hand side) and the data with "perturbative removal of the lattice artifacts" (right-hand side) are shown. The point at $a/L = 0$ in (b) indicates the extrapolated value for the Iwasaki action obtained by the constrained fit whose fitting function is represented by the dotted lines. The point at $a/L = 0$ in (d) indicates the extrapolated value for the LW action obtained by the linear fit whose fitting function is shown as a dotted line, for the data of one-loop O(a) improved action.

TABLE VI. One-loop deviations for various gauge actions and with k-level O(a) improvement.

	Iwasaki action			LW action	
L/a	$\delta_1^{(0)}$	$\delta_1^{(1A)}$	$\delta_1^{(1B)}$	$\delta_1^{(0)}$	$\delta_1^{(1A)}$
4	−0.020 96	0.017 00	0.015 77	0.003 278	0.002 536
6	−0.019 22	0.006 08	0.005 92	0.000 911	0.000 417
8	−0.014 99	0.003 99	0.003 95	0.000 527	0.000 156
12	−0.010 64	0.002 01	0.002 00	0.000 296	0.000 049

agree in the continuum limit $\sigma^{(k)}(2, u) = \sigma(2, u)$. The fit has a good $\chi^2/N_{\text{d.o.f.}}$ as listed in Table VII.

As shown in Fig. 2(c), the scaling violations are quite small for the LW action. This is consistent with the fact found in Ref. [16] that the lattice artifacts are quite small at one loop. Moreover, the difference between the tree-level and one-loop O(a) improvement is invisible in this precision, as a result of the smallness of the improvement coefficients $c_t^{P(1)}$ and $c_t^{R(1)}$. As shown in Fig. 2(d), the perturbative removal of lattice artifacts has almost no effect except for $L/a = 4$, since $\delta_1^{(k)}(2, a/L)$ with $L/a =$ 6, 8, and 12 is quite small. In Table VII we quote the extrapolated value for the LW action, obtained by a linear fit to data of the one-loop O(a) improved action with the perturbative removal of lattice artifacts. For comparison the results of the ALPHA Collaboration are also included [17].

Results at the strong coupling $u = 2.4484$ are plotted in Fig. 3. For the Iwasaki action, the one-loop O(a) improvement shows large lattice artifacts for both conditions A and B, particularly for the coarse lattice [see Fig. 3(a)]. As shown in Fig. 3(b), the perturbative removal of lattice artifacts well reduces the scaling violation in the case of condition B, but it still remains rather large for condition A. Therefore, we include a quadratic term in the fitting form,

$$\Sigma_1^{(k)}(2, u, a/L) = \sigma^{(k)}(2, u) + \omega_1^{(k)}(u)a/L + \omega_2^{(k)}(u)(a/L)^2, \tag{4.5}$$

for the data of $k = 1A$ and $1B$, while we use the linear fitting form Eq. (4.4) for the data of $k = 0$. The extrapolated values obtained with the constraint $\sigma^{(k)}(2, u) = \sigma(2, u)$ for a unique continuum value are listed in Table VII. We note that $|\omega_2^{(1A)}(u)/\omega_1^{(1A)}(u)| \approx O(10)$ in the fit for condition A. This suggests that condition A accidentally enhances the coefficient of the O(a^2) term. It does not necessarily mean, however, that the one-loop O(a) improvement itself is inefficient at this coupling constant. Indeed the one-loop O(a) improvement with condition B shows good scaling behavior. As for the LW action, Figs. 3(c) and 3(d) show that neither the one-loop O(a) improvement nor the perturbative removal works effectively. Concerning the extrapolation we simply use the same procedure as in the weak coupling case, i.e., the linear fitting form to the perturbative removal data for one-loop O(a) improvement. The result is given in Table VII.

We observe in Table VII that the three values obtained with the Iwasaki and LW action in the present work and that of the ALPHA Collaboration [17] at the weak coupling are consistent within 1σ. At the strong coupling, the value for the LW action undershoots relative to the others by 1.5–2σ. We think that the latter disagreement is caused by a large lattice artifact for the LW action, which makes the choice of the fitting form difficult. For example, if we assume that O(a) errors for the LW action are negligible, we can obtain a result consistent with the values of the other actions within 1σ, by using a purely quadratic fitting form. Further investigation is needed to clarify this point.

B. Low energy scale ratio

We now combine $L_{\max}/a$ and a/r_0 for the Iwasaki action to form the ratio $L_{\max}/r_0$ and extrapolate it to the continuum limit:

$$L_{\max}/r_0 = \lim_{a/L_{\max}\to 0} (L_{\max}/a) \times (a/r_0). \tag{4.6}$$

In the fourth column of Table VIII, we give the first factor, which is taken from Table IV; the error of $L_{\max}/a$ is estimated by propagating that of $\bar{g}^2_{\text{SF}}(L_{\max})$.

The second factor r_0/a is given in the third column of Table VIII. This is obtained by an interpolation of the results for r_0/a in Table IX using a polynomial [31]

$$\ln(a/r_0) = c_1 + c_2(\beta - 3) + c_3(\beta - 3)^2. \tag{4.7}$$

The fit, plotted in Fig. 4, gives

$$c_1 = -2.193(6), \quad c_2 = -1.344(7), \quad c_3 = 0.191(24), \tag{4.8}$$

with $\chi^2/N_{\text{d.o.f.}} = 4.10/6$ in the range $2.456 \le \beta \le 3.53$.

TABLE VII. The extrapolated values of the SSF with various gauge actions for both the weak and the strong couplings. The values in the case of the plaquette action are quoted from the reference as indicated.

Action	$\sigma(2, u = 0.9944)$	$\chi^2/N_{\text{d.o.f.}}$	$\sigma(2, u = 2.4484)$	$\chi^2/N_{\text{d.o.f.}}$
Iwasaki	1.107(3)	1.5/8	3.485(34)	1.9/6
LW	1.111(4)	2.0/2	3.410(30)	0.1/2
Plaquette [17]	1.110(11)	3.3/2	3.464(40)	0.9/4

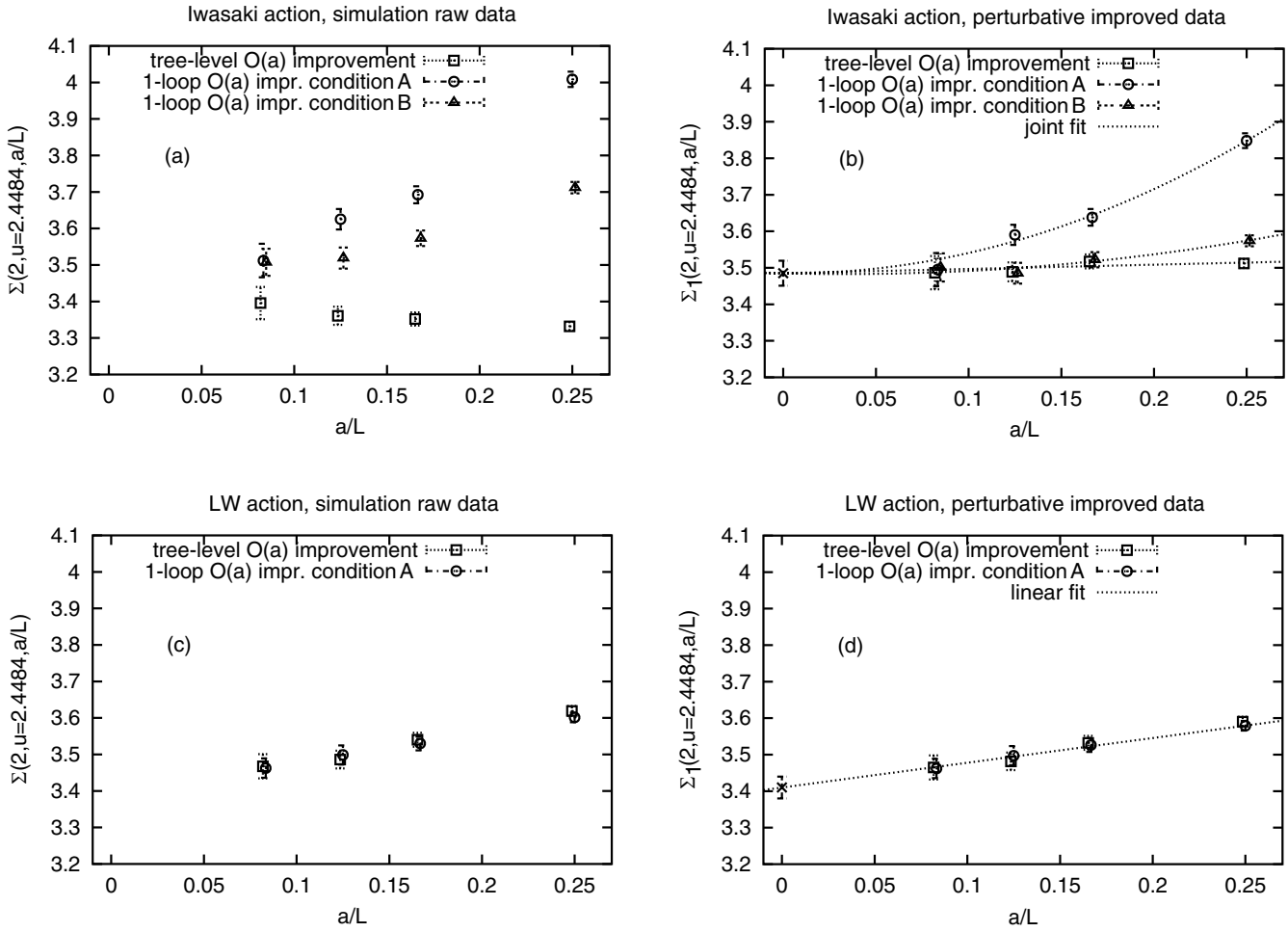

FIG. 3. Results of SSF at the strong coupling $u = 2.4484$ with the various gauge actions. Concerning the symbols and the lines, the same explanation as the weak coupling case is followed.

The error of r_0/a in Table VIII includes both statistical and systematic ones. We take the central value of r_0/a from the result of the fit above and estimate the systematic error from the difference of r_0/a between the central value and the result of another fit including a $c_4(\beta - 3)^3$ term.

The combination of the two factors for various β values are listed in the fifth column in Table VIII. The

TABLE VIII. The low energy scale at various values of β for the Iwasaki action.

Degree of O(a) improvement	β	r_0/a	$L_{\max}/a$	$L_{\max}/r_0$
Tree	2.7000	5.886(26)	4.000(11)	0.680(4)
	3.0057	9.03(12)	6.000(35)	0.664(10)
	3.2154	11.87(19)	8.000(41)	0.674(12)
	3.5219	17.16(14)	12.00(8)	0.699(7)
	2.4594	4.098(12)	4.000(9)	0.976(4)
One-loop	2.8556	7.352(59)	6.000(33)	0.816(8)
condition A	3.1047	10.29(16)	8.000(31)	0.777(12)
	3.4496	15.78(16)	12.00(7)	0.761(9)
	2.5382	4.625(12)	4.000(8)	0.865(3)
One-loop	2.8921	7.735(73)	6.000(28)	0.776(8)
condition B	3.1376	10.74(17)	8.000(38)	0.745(12)
	3.4734	16.22(15)	12.00(7)	0.740(8)

TABLE IX. β versus r_0/a with the Iwasaki action. The values of r_0/a are taken from the references quoted in the last column.

β	r_0/a	Reference
2.456	4.080(16)	[29]
2.461	4.089(14)	[28]
2.487	4.286(15)	[29]
2.528	4.570(21)	[29]
2.575	4.887(16)	[29]
2.659	5.556(30)	[28]
3.000	8.88(13)	In this work
3.200	11.53.(15)	[27]
3.530	17.35(13)	In this work

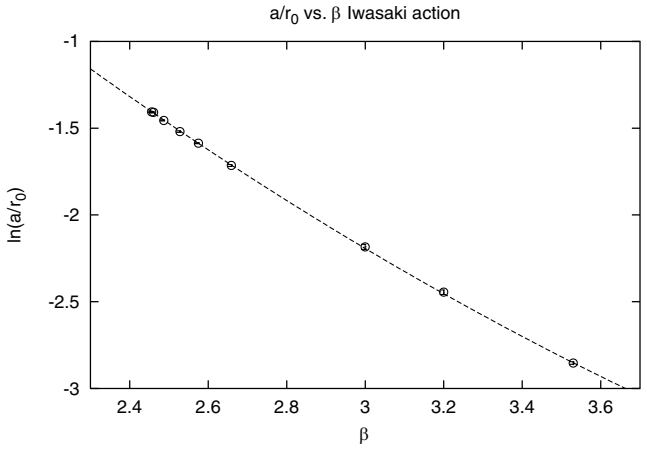

FIG. 4. Interpolation of r_0/a with phenomenological representation [Eq. (4.7)] in the range $2.456 \leq \beta \leq 3.53$.

β dependence of $L_{\max}/r_0$ can be considered as lattice cutoff effects. For an extrapolation to the continuum limit, we use a fit form

$$a/r_0 = b_1 a/L_{\max} + b_2(a/L_{\max})^2 + b_3(a/L_{\max})^3, \quad (4.9)$$

where $b_i (i = 1, 2, 3)$ are fit parameters and b_1 is the continuum value of the low energy scale ratio, rather than fitting $L_{\max}/r_0$ as a function of $a/L_{\max}$. In this way one can avoid the correlation of errors which complicates the latter fit.[1] We apply Eq. (4.9) to three sets of data, i.e., data for the tree-level O(a) improvement and those of the one-loop O(a) improvement with the conditions A and B. For the first set of data, we set $b_3 = 0$ (a linear fit) and exclude the point at $a/L = 1/4$. An alternative fit including that point and allowing a nonzero b_3 yields a consistent value for b_1 within errors. However, we think that the fit is not so reliable since $\chi^2/N_{\text{d.o.f.}}$ is too small and the linear terms are rather large. Therefore we exclude the point and use the linear fit for the remaining three points. In Fig. 5 $L_{\max}/r_0$ is plotted as a function of $a/L_{\max}$. Dashed lines are the fit curves Eq. (4.9) divided by $a/L_{\max}$, and the point at $a/L_{\max} = 0$ shows the extrapolated value b_1.

The extrapolated value is given in Table X, together with the previous result for the standard Wilson plaquette action [18]. While rather large lattice artifacts are observed for both standard Wilson plaquette action and Iwasaki action, the extrapolated values agree within errors.

V. CONCLUSIONS AND DISCUSSIONS

In this paper, we have calculated the SSF at the weak and the strong couplings for both Iwasaki and LW actions with the one-loop O(a) improved as well as the tree-level O(a) improved boundary terms. We have also calculated the low energy scale ratio for the Iwasaki action with both tree-level and one-loop O(a) improvements. The extrapolated values of the SSF at the weak and strong couplings for various gauge actions are consistent within 1σ and 2.3σ, respectively. The low energy scale ratio is also consistent between the Iwasaki and plaquette actions within 1σ. In conclusion, we have confirmed the universality of both quantities.

We have investigated lattice cutoff effects in some detail. In the extrapolation procedure, the perturbative removal of lattice artifacts reduces the scaling violation of the SSF for the Iwasaki action with the tree-level O(a) improvement and the one-loop O(a) improvement with condition B. Indeed, at the strong coupling at the coarsest lattice $L/a = 4$, cutoff effects are of order 1% and 3%, respectively, if one compares the extrapolated value

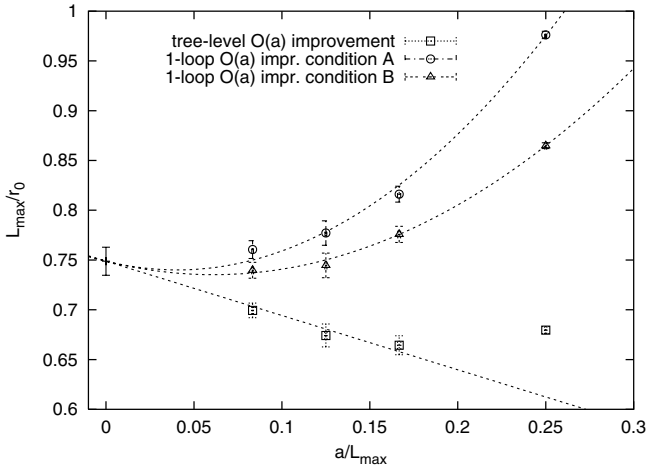

FIG. 5. Cutoff dependence of $L_{\max}/r_0$ for some choices of the boundary counterterms with the Iwasaki action. The errors on the x axis are invisible in this scale. The constrained fit is represented by dotted lines. In the fit the points at $a/L_{\max} = 1/4$ of the tree-level O(a) improvement are not included.

[1]Since the error on $L_{\max}/a$ is small, one may perform a continuum extrapolation of $L_{\max}/r_0$ as a function of $a/L_{\max}$ neglecting the error on the x axis. We observe consistency between the two methods.

TABLE X. The extrapolated values of the low energy scale ratio with various gauge actions. The values in the case of the plaquette action are quoted from the reference as indicated.

Action	$L_{\max}/r_0$	$\chi^2/N_{\text{d.o.f.}}$
Iwasaki	0.749(14)	3.93/5
Plaquette [18]	0.738(16)	

obtained by the constrained fit. At the weak coupling, they are roughly 1% for both cases. We conclude that for the Iwasaki gauge action these combinations of improvements are the good choice for controlling lattice artifacts. This conclusion is also supported by the fact that an individual extrapolation to the continuum limit with the linear fitting form for the data set with the tree-level O(a) improvement or the one-loop O(a) improvement with condition B gives a result consistent with the extrapolated value estimated from the constrained fit within errors, at both weak and strong couplings.

As mentioned in the Introduction, this work is the second step toward $N_{\text{f}} = 2$ and 3 simulations. The present study shows that we should use the tree-level O(a) improved action or the one-loop O(a) improved action with condition B in future simulations with dynamical quarks.

ACKNOWLEDGMENTS

This work is supported in part by the Grant-in-Aid of the Ministry of Education (No. 13135204, No. 13640260, No. 14046202, No. 14740173, No. 15204015, No. 15540251, No. 15540279, No. 15740134, No. 16028201, No. 16540228, No. 16740147, No. 16·11968). S.T. is supported by the JSPS Research Fellowship.

[1] Particle Data Group Collaboration, K. Hagiwara *et al.*, Phys. Rev. D **66**, 010001 (2002).
[2] M. Lüscher, R. Narayanan, P. Weisz, and U. Wolff, Nucl. Phys. **B384**, 168 (1992).
[3] S. Sint, Nucl. Phys. **B421**, 135 (1994).
[4] M. Lüscher, S. Sint, R. Sommer, P. Weisz, and U. Wolff, Nucl. Phys. **B491**, 323 (1997).
[5] K. Jansen and R. Sommer, Nucl. Phys. **B530**, 185 (1998).
[6] M. Lüscher, S. Sint, R. Sommer, and H. Wittig, Nucl. Phys. **B491**, 344 (1997).
[7] M. Guagnelli, J. Heitger, R. Sommer, and H. Wittig, Nucl. Phys. **B560**, 465 (1999).
[8] ALPHA Collaboration, A. Bode *et al.*, Phys. Lett. B **515**, 49 (2001).
[9] ALPHA Collaboration, M. Della Morte *et al.*, Nucl. Phys. B, Proc. Suppl. **119**, 439 (2003).
[10] JLQCD Collaboration, S. Aoki *et al.*, Nucl. Phys. B, Proc. Suppl. **106**, 1079 (2002).
[11] JLQCD Collaboration, S. Aoki *et al.*, Nucl. Phys. B, Proc. Suppl. **106**, 263 (2002).
[12] CP-PACS Collaboration, S. Aoki *et al.*, Nucl. Phys. B, Proc. Suppl. **119**, 433 (2003).
[13] CP-PACS/JLQCD Collaboration, K-I. Ishikawa *et al.*, Nucl. Phys. B, Proc. Suppl. **129**, 444 (2004).
[14] CP-PACS/JLQCD Collaboration, T. Kaneko *et al.*, Nucl. Phys. B, Proc. Suppl. **129**, 188 (2004).
[15] Y. Iwasaki, Nucl. Phys. **B258**, 141 (1985); University of Tsukuba Report No. UTHEP-118, 1983 (unpublished).
[16] S. Takeda, S. Aoki, and K. Ide, Phys. Rev. D **68**, 014505 (2003).
[17] ALPHA Collaboration, S. Capitani *et al.*, Nucl. Phys. **B544**, 669 (1999).
[18] S. Necco and R. Sommer, Nucl. Phys. **B622**, 328 (2002).
[19] M. Lüscher, R. Sommer, P. Weisz, and U. Wolff, Nucl. Phys. **B413**, 481 (1994).
[20] T. Klassen, Nucl. Phys. **B509**, 391 (1998).
[21] M. Lüscher and P. Weisz, Nucl. Phys. **B240**, 349 (1984).
[22] S. Aoki, R. Frezzotti, and P. Weisz, Nucl. Phys. **B540**, 501 (1999).
[23] M. Lüscher and P. Weisz, Commun. Math. Phys. **97**, 59 (1985); **98**, 433(E) (1985); Phys. Lett. **158B**, 250 (1985).
[24] R. Sommer, Nucl. Phys. **B411**, 839 (1994).
[25] M. Lüscher, P. Weisz, and U. Wolff, Nucl. Phys. **B359**, 221 (1991).
[26] B. Gehrmann, Ph.D. thesis, Humboldt University (hep-lat/0207016).
[27] CP-PACS Collaboration, M. Okamoto *et al.*, Phys. Rev. D **60**, 094510 (1999).
[28] CP-PACS Collaboration, A. Ali Khan *et al.*, Phys. Rev. D **64**, 114501 (2001).
[29] CP-PACS Collaboration, A. Ali Khan *et al.*, Phys. Rev. D **65**, 054505 (2002).
[30] ALPHA Collaboration, G. de Divitiis *et al.*, Nucl. Phys. **B437**, 447 (1995).
[31] ALPHA Collaboration, M. Guagnelli, R. Sommer, and H. Wittig, Nucl. Phys. **B535**, 389 (1998).